Archaeometric analysis of patinas of the outdoor copper statue Sant'Oronzo (Lecce, Italy) preparatory to the restoration

Archaeometric analysis of *patinas* of the outdoor copper statue *Sant'Oronzo* (Lecce, Italy) preparatory to the restoration

Giovanni Buccolieri[a], Alfredo Castellano[a], Antonio Serra[a], Giorgio Zavarise[b], Elisabetta Palmiero[c], Alessandro Buccolieri[d,*]

[a] Dipartimento di Matematica e Fisica, University of Salento, Lecce, Italy
[b] Dipartimento di Ingegneria Strutturale, Edile e Geotecnica, Politecnico di Torino, Torino, Italy
[c] Restauratrice dell'Azienda Colaci Emilio, Impianti e Restauri, Alessano, Lecce, Italy
[d] Dipartimento di Scienze e Tecnologie Biologiche e Ambientali, University of Salento, Lecce, Italy

[*] Corresponding author. A. Buccolieri, Dipartimento di Scienze e Tecnologie Biologiche e Ambientali, University of Salento, Lecce, Italy. E-mail: alessandro.buccolieri@unisalento.it

Abstract

The *Sant'Oronzo* statue (Lecce, Southern Italy) consists of an internal wooden structure, completely covered with copper sheets, lying on a concrete base about 1.5 meters high, which is placed on the top of a Roman column about 29 meters high. Lecce may be classified as urban site since it is mainly influenced by vehicular traffic and it is not affected by intense industrial emissions.
In the time schedule of the restoration, first of all, non-destructive analyses were planned. In particular, a portable energy dispersive X-ray fluorescence (ED-XRF) was used in order to map the composition of the *patinas* and to evaluate their degradation. Subsequently, a micro-sampling was performed both of the statue and the column. The collected samples were analysed by using Raman spectroscopy and X-Ray Diffraction in order to evaluate chemical composition.
This paper summarizes the archaeometric results and the diagnostic information obtained before of the restoration, which are significant for the restorers' subsequent work.

Keyword: outdoor statue, copper, *patina*, ED-XRF, Raman, XRD

1. Introduction

The *patina* of outdoor copper manufact has different chemical composition depending on the several parameters such as alloy composition, environmental conditions (for instance, urban, rural, marine, industrial), location of statue (in exposed areas or sheltered areas) and exposure time [1–4]. In

particular, in urban atmospheres, *patinas* directly exposed to rain are unstable and are leachable by rainwaters.

The *patinas* spontaneously develop over time on copper and bronze surfaces due to chemical reactions with the environment, creating corrosion compounds with various color (for example green, red, bluish, brown and black) and different composition such as copper oxide, copper sulfide, copper chloride, copper sulfate and copper carbonate [5–9]. In particular, the degradation compounds most commonly found in copper manufacts are Cu_2O (cuprite), CuO (tenorite), Cu_2S (chalcocite), CuS (covellite), CuCl (nantokite), $CuCl_2{\cdot}2H_2O$ (eriochalcite), $Cu_2Cl(OH)_3$ (atacamite), $Cu_2Cl(OH)_3$ (botallackite), $Cu_2Cl(OH)_3$ (clinoatacamite), $Cu_3SO_4(OH)_4$ (antlerite), $Cu_4SO_4(OH)_6$ (brochantite), Cu_2OSO_4 (dolerophanite), $Cu_4SO_4(OH)_6{\cdot}2H_2O$ (langite), $Cu_4SO_4(OH){\cdot}6H_2O$ (posnjakite), $Cu_4SO_4(OH){\cdot}2H_2O$ (wroewulfite), $Cu_2(CO_3)(OH)_2$ (malachite), $Cu_3(CO_3)_2(OH)_2$ (azurite) [10–12]. Jambor *et al.,* 1996 [13] reported for the first time the clinoatacamite, a new mineral polymorph of $Cu_2Cl(OH)_3$. Therefore, previous reports on paratacamite should probably be assigned to clinoatacamite instead. The polymorphs $Cu_2Cl(OH)_3$ (atacamite, paratacamite and clinoatacamite), in combination with different hydroxy sulfates and cuprite, are dominant in the black sheltered areas, while rain-washed green areas mainly consist of brochantite and cuprite [5,14,15].

The chemical composition of alloy and *patina* of copper or bronze can be determined using various analytical methods such as energy dispersive X-ray fluorescence (ED-XRF), Raman spectroscopy, scanning electron microscopy-energy dispersive X-ray (SEM-EDX), X-ray diffraction (XRD) and atomic absorption spectroscopy (AAS). Nevertheless, methodologies often favoured in the field of cultural heritage are non-destructive and portable techniques.

This work describes the experimental results of the diagnostic analysis performed on the *Sant'Oronzo* statue (Lecce, Southern Italy) before starting the restoration in June 2018.

Lecce (40° 21' N; 18° 10' E; 30 m above sea level) has about 95 thousand inhabitants and it is about 20 km away from both the Adriatic Sea and Ionian Sea. The town may be classified as urban site since it is mainly influenced by vehicular traffic [16,17]. Fig. 1 shows some photos of the statue, which highlight serious state of degradation of the copper sheet, of the Roman column and of the concrete base.

2. Materials and methods

2.1. Description of statue

The *Sant'Oronzo* statue was built in Venice in 1739 and it is 4.90 meters high. It has an internal wooden structure, completely covered with copper sheets, which were held together by copper nails.

The thickness of copper sheets is equal to about 1 mm. The original copper nails are about 2 to 5 cm long (Fig. S1).

The statue is placed in *Sant'Oronzo* square, in the center of Lecce (Southern Italy), on a recent concrete base (2.65 m × 2.65 m) about 1.5 meters high, which is positioned on a Roman column about 29 meters high. The bottom of the statue is covered with a sheet of lead, which sit on the concrete base.

The last restoration was performed in years 1982 to 1987. In the last restoration, several copper rivets (with a steel nail, see Fig. S2) have been added to keep together the copper foils (Fig. S3). Unfortunately, the use of these rivets induced galvanic corrosion phenomena, which are visible to the naked eye. In fact, a close visual examination of statue allows to highlight two principal typologies of *patinas*: light green *patina* (in areas exposed to leaching) and dark *patina* (in areas not exposed to leaching), in addition to the numerous red drips, in correspondence of the rivets. Moreover, the column shows both green and dark dripping on concrete basement and on Roman capital.

On January 30, 2019 the statue was removed and transferred for restoration to *Palazzo Carafa*, the municipal building of Lecce, nearby the original site. Fig. S4 shows a picture of the statue in the room where it will be restored.

2.2. Methods

2.2.1 ED-XRF

EDXRF portable equipment, which was assembled in our laboratory, is composed by an X-ray tube (MOXTEK Inc., USA) with palladium anode air-cooled and by a detector Si-PIN (Amptek Inc., USA). The detector has a resolution of energy of about 180 eV at 5.9 keV. The output of the X-ray tube is collimated and the analyzed area has a diameter of about 3 mm [18,19]. For each measuring point, three EDXRF spectra were acquired, with acquisition time of 60 seconds and with a tube voltage of 6 kV at 40 μA and of 20 kV at 3 μA.

Five standard samples, with known chemical compositions, were used to calibrate the apparatus and to obtain reliable experimental data. For standards preparation, copper (II) sulphate pentahydrate ($CuSO_4 \cdot 5H_2O$), copper (II) chloride dihydrate ($CuCl_2 \cdot 2H_2O$), copper (I) oxide (Cu_2O), copper (II) sulfide (CuS) and iron powder have been used. All chemical compounds were purchased from Sigma-Aldrich® with analytical grade.

Each standard was prepared by mixing the compounds in different weight percentages. The use of different compounds with the same elements, but in different oxidation state, is irrelevant from the point of view of the XRF analysis, but has allowed to obtain the calibration samples at different

concentrations. In particular, the chemicals compounds have been weighted by using an analytical balance KERN model ABT 100-5M, subsequently mixed and homogenized in an agate mortar for ten minutes and finally compressed at 200 bar for ten minutes. The homogeneity of elements in the standard meets the requirements for the EDXRF quantitative analysis. Moreover, the samples analysed are supposed to "*infinite thickness*" and therefore the quantitative results are expressed in terms of weight percentage (% wt).

Copper, sulphur, chlorine and iron were determined, for each measurement point, in order to individuate the chemical composition of the *patinas*. The description of each measurement point is summarized in Table 1. The values of detection limit, all reported in wt %, for copper, sulphur, chlorine and iron are equal to 1.0, 0.5, 0.5 and 0.5 respectively. The software Microcal Origin Professional® has been used to elaborate the experimental data obtained [20].

2.2.2 Raman spectroscopy

Raman analysis was performed on seven samples to identify *patina* composition. Fig. 1 shows the sampling point of each sample whose characteristics are described in Table 2. The samples were pounded to a fine powder in an agate mortar, homogenized and subsequently analyzed. Raman analyses were achieved by using a spectrometer Renishaw model Invia (spectral resolution: 0.5 cm^{-1}; spectral range: 100 – 3700 cm^{-1}) with an argon-ion laser (λ = 514.5 nm) and a LEICA metallographic microscope. The laser beam was focused on the sample with 15 mW of excitation power. The spectra were acquired for 20 accumulations by 100 s and repeated on five different points. Then an average of Raman spectra was obtained. The spectra were obtained with baseline correction and compared with standard spectra from the database www.rruff.info (atacamite R050098, brochantite R060133, calcite R040170, cuprite R050384, graphite R050503, gypsum R040029, murdochite R110122).

2.2.3 XRD

The XRD analyses were performed on the same samples examined with Raman spectroscopy. The samples were analysed by using a diffractometer Rigaku model Mini Flex with Cu-K_α radiation (λ = 0.154 nm). The measurements were carried out with 30 kV accelerating voltage, 15 mA current, scan angle in 2θ from 10° to 80°, with step size of 0.01° and scan speed of 0.05°·s^{-1}. Three scans for each measurement were performed. XRD patterns were manually compared with standards XRD patterns from the database www.rruff.info (atacamite R050098, brochantite R060133, calcite R040170, cuprite R050384, graphite R050503, gypsum R040029, murdochite R110122).

3. Result and Discussion

3.1 ED-XRF analysis

Experimental results of ED-XRF analysis carried out on the *patinas* of the *Sant'Oronzo* statue are summarized in Table 1.

Green *patina*, exposed to leaching (sample n. 01), shows copper (65±2 % wt) as main element and sulphur (20±2 % wt) as secondary element. Green *patina* on the mantle (sample n. 09) and the greenish dripping on the right arm (sample n. 06) have different composition.

Dark *patinas*, not exposed to leaching (samples n. 05, 07, 10, 11, 13 and 15), shows copper as main element and chlorine as secondary element. Moreover, the dark *patina* with red dripping on the bottom right mantle (sample n. 12) shows higher sulphur concentration (11.5±1.0 % wt) and iron (1.5±0.5 % wt) as in trace element. Red *patinas*, exposed to leaching (samples n. 02, 03 and 04), show copper and iron as main element and sulphur as secondary element.

It is important to note that iron is widely present on the surface of statue as minor element or in trace. This is due to the corrosion of the rivets nails added during the last restoration accomplished from 1982 to 1987. In fact, the recent rivet (sample n. 19) shows copper (39±2 % wt) as main element and iron (10.0±1.0 % wt) as secondary element, whereas the rivet (sample n. 20) shows iron (27±2 % wt) as main element and copper (12.0±1.0 % wt) as secondary element.

The original nails show copper (45-56 % wt) as main element. Moreover, the nail n. 16 and n. 18 show chlorine (21±2 % wt) as secondary element, while the nail n. 17 shows sulphur (12.0±1.0 % wt) and chlorine (5.0±0.5 % wt) as secondary elements.

Cleaning tests were also carried out on some measuring points both on areas of the statue (sample n. 01 and n. 15) and on nails (sample n. 16, n. 17 and n. 18) and on rivets (sample n. 19). In any case, the increase of copper concentration was highlighted with a simultaneous decrease in sulphur and chlorine concentration.

3.2 Raman and XRD analysis

Raman spectroscopy offers chemical identification of compounds in order to discriminate the corrosion products of copper or bronze manufact [6,21–25]. In particular, the Raman signals of copper hydroxychlorides and copper hydroxysulphates can be observed in two main regions: the first at lower wavenumbers, between 100 cm^{-1} and 1100 cm^{-1}, includes Cu–O deformation, Cu–Cl deformation and SO_4^{2-} deformation. The second, at high wavenumbers, between 3000 cm^{-1} and 3700

cm^{-1}, includes the Cu–O–H stretching vibrations. In particular, the number of bands in this region usually reflects the number of different O–H groups present in the structure, except in the case of strong overlap of the bands. For instance, brochantite ($Cu_4SO_4(OH)_6$) has six hydroxyl groups bonded to adjacent sulphate group, and therefore Raman spectroscopy shows six peaks. There is another region, between 1100 cm^{-1} and 3700 cm^{-1}, which includes the signals that characterize the amorphous carbon [26–28], often determined on outdoor copper monuments, as well as C–H vibrations of organic compounds and the water features present in several hydrated mineral phases.

In Table 3 it was tried to assign the type of deformation for each Raman signal obtained in analysed *patinas* of the statue.

Fig. 2a shows the comparison between the Raman spectrum of the green *patina* and of the standard brochantite. Raman spectrum of green *patina* has the following signals: 120, 140, 200, 242, 318, 390, 420, 450, 485, 506, 595, 609, 622, 910, 975, 1075, 1095, 1125, 1350, 1580, 3265, 3375, 3402, 3489, 3565, 3588 cm^{-1}. According to the data reported by scientific literature [29–35] all signals of green *patina* are attributable to brochantite, except two peaks broader with Raman shift values of about 1350 cm^{-1} and 1580 cm^{-1}, which are attributable to amorphous carbon and are called D (disorder band) and G (graphitic band) band, respectively. Moreover, the spectrum of green *patina* shows a broad band in the range 2800–3000 cm^{-1}, which is the region of C–H vibrations of saturated organic molecules, mainly hydrocarbons and carboxylic acids.

Fig. 3a shows the comparison between the Raman spectrum of the dark *patina* and of the standard atacamite ($Cu_2Cl(OH)_3$). Raman spectrum of dark *patina* has the following signals: 220, 415, 510, 635, 810, 905, 980, 1340, 1600, 2915, 3200, 3355, 3435 cm^{-1}. In according to the data reported by scientific literature, all signals of dark *patina* are attributable to atacamite, in addition to the presence of amorphous carbon. Moreover, the spectrum shows two broad bands in the range 2800–3000 cm^{-1}, which are the region of C–H vibrations of saturated organic molecules, mainly hydrocarbons and carboxylic acids.

Fig. 4a shows the comparison between the typical Raman spectrum of the sample C04 (green dripping on Roman capital, West side) and of the standard calcite ($CaCO_3$). Raman spectrum of sample C04 has the following signals: 155, 285, 715, 1085, 1435, 1750, 2625, 2670, 3220 and 3470 cm^{-1}. This comparison demonstrated that the sample is mainly composed of calcite and the signals relating C–H vibrations of saturated organic molecules.

XRD analysis prove that both the green *patina* (Fig. 2b) and the dark *patina* (Fig. 3b) contain cuprite (2θ equal to 29.6, 36.5, 42.3, 61.4, 73.5 and 77.4). This oxide represents the protective layer that normally covers outdoor copper and bronze monuments. In addition, green *patina* is characterized by the presence of brochantite, whereas dark *patina* is characterized mainly by the presence of atacamite more brochantite.

Several studies have shown that brochantite is converted into atacamite in solutions containing high levels of chloride ions through a mechanism of dissolution and precipitation. This chemical-physical process is reasonable considering the different solubility of the two compounds and their stability ratio:

$$Cu_4(OH)_6SO_4 \leftrightarrows 4\ Cu^{2+} + 6\ OH^- + SO_4^{2-}\ (pK_{s\ brochantite} = -68.9)$$

$$Cu_4(OH)_6C1_2 \leftrightarrows 4\ Cu^{2+} + 6\ OH^- + 2\ Cl^-\ (pK_{s\ atacamite} = -69.8)$$

$$Cu_4(OH)_6SO_4 + 2\ Cl^- \leftrightarrows Cu_4(OH)_6C1_2 + SO_4^{2-}\ (pK_{\ brochantite/atacamite} = -0.929)$$

XRD pattern of the sample C01 (dark dripping on concrete pulvino) shows the presence mainly of calcite and gypsum, typical compounds used in cementitious material in the form of powders, and of murdochite (Cu_6PbO_8). Fig. S5 shows the XRD spectrum of sample C01. The existence of murdochite on pulvino can be justified considering the corrosion of the lead plate placed at the pedestal of the statue on which the wooden structure rests.

XRD pattern of the sample C02 (green dripping on concrete pulvino) shows the presence mainly of calcite. The weak signal at 2θ equal to 16.2° is due to atacamite, confirming that its drip from the copper statue is the cause of the green coloured areas. The sample C03 (dark dripping on Roman capital) is also characterized by the presence of calcite as main phase. The dark colour is due both to the presence of carbon particles and to a dripping of murdochite that comes from the statue's pedestal. The sample C04 (green dripping on Roman capital) is mainly characterized by calcite (Fig. 4b). The light green colouring on the capital could be due to brochantite of coming from the metallic statue.

The sample C05 (dark area not exposed to washouts on Roman capital) shows the presence of gypsum as the main phase and calcite. The graphite signal is also present and this may be due to carbon particles deposited in not washed region, which determine the dark colour.

The results obtained by using XRD confirm the results obtained by Raman spectroscopy.

4. Conclusion

Green *patinas* were constituted mainly by cuprite and brochantite, while dark *patinas* were constituted mainly by cuprite, brochantite and atacamite. The presence of atacamite in areas not directly exposed to rain may be due probably to deposits of marine spray accumulated in these sheltered regions of the statue.

Furthermore, all the *patinas* contain amorphous carbon which demonstrates the presence of carbon deposits. In particular, the highest concentration of amorphous carbon was detected in the sheltered dark *patinas*.

The improper use of the rivets used in the last restoration from 1982 to 1987 has irreversibly damaged the analysed monument, thus modifying its aesthetics (with evident red areas around each rivet and red dripping starting from the rivet).

The simultaneous use of the analytical techniques has allowed to define the compounds of degradation of *patinas* and the information obtained was of fundamental importance for the subsequent work of the restorers.

Acknowledgments

The authors thank Massimo Luggeri (Dipartimento di Scienze e Tecnologie Biologiche e Ambientali, Università del Salento), who has contributed to improving the quality of the figures. We are grateful to Company Colaci Emilio Impianti e Restauri (Alessano, Lecce, Italy) and the restorer Elisabetta Palmiero for promoting this study and for his continuous collaboration. We are also very grateful to Arch. Maria Piccarreta (*Soprintendenza archeologia belle arti e paesaggio per le province di Brindisi, Lecce e Taranto*) for her always collaborative attitude.

References

[1] G.M. Ingo, T. De Caro, C. Riccucci, E. Angelini, S. Grassini, S. Balbi, P. Bernardini, D. Salvi, L. Bousselmi, A. Çilingiroğlu, M. Gener, V.K. Gouda, O.A.L. Jarrah, S. Khosroff, Z. Mahdjoub, Z.A.L. Saad, W. El-Saddik, P. Vassiliou, Large scale investigation of chemical composition, structure and corrosion mechanism of bronze archeological artefacts from Mediterranean basin, Appl. Phys. A Mater. Sci. Process. 83 (2006) 513–520. doi:10.1007/s00339-006-3550-z.

[2] D.E. Couture-Rigert, P.J. Sirois, E.A. Moffatt, An investigation into the cause of corrosion on indoor bronze sculpture, Stud. Conserv. 57 (2012) 142–163. doi:10.1179/2047058412Y.0000000004.

[3] X. Zhang, I. Odnevall Wallinder, C. Leygraf, Mechanistic studies of corrosion product flaking on copper and copper-based alloys in marine environments, Corros. Sci. 85 (2014) 15–25. doi:10.1016/j.corsci.2014.03.028.

[4] G. Masi, J. Esvan, C. Josse, C. Chiavari, E. Bernardi, C. Martini, M.C. Bignozzi, N. Gartner, T. Kosec, L. Robbiola, Characterization of typical patinas simulating bronze corrosion in outdoor conditions, Mater. Chem. Phys. 200 (2017) 308–321. doi:10.1016/j.matchemphys.2017.07.091.

[5] R.A. Livingston, Influence of the Environment on the Patina of the Statue of Liberty, Environ. Sci. Technol. 25 (1991) 1400–1408. doi:10.1021/es00020a006.

[6] W. Martens, R.L. Frost, J.T. Kloprogge, P.A. Williams, Raman spectroscopic study of the basic copper sulphates - Implications for copper corrosion and "bronze disease," J. Raman Spectrosc. 34 (2003) 145–151. doi:10.1002/jrs.969.

[7] R.L. Frost, P.A. Williams, J.T. Kloprogge, W. Martens, Raman spectroscopy of the copper chloride minerals nantokite, eriochalcite and claringbullite – implications for copper corrosion, Neues Jahrb. Für Mineral. - Monatshefte. 2003 (2003) 433–445. doi:10.1127/0028-3649/2003/2003-0433.

[8] V. Hayez, V. Costa, J. Guillaume, H. Terryn, A. Hubin, Micro Raman spectroscopy used for the study of corrosion products on copper alloys: Study of the chemical composition of artificial patinas used for restoration purposes, Analyst. 130 (2005) 550–556. doi:10.1039/b419080g.

[9] X.D. Liu, D.D. Meng, X.G. Zheng, M. Hagihala, Q.X. Guo, Mid-IR and Raman Spectral Properties of Clinoatacamite-Structure Basic Copper Chlorides, Adv. Mater. Res. 146–147 (2010) 1202–1205. doi:10.4028/www.scientific.net/AMR.146-147.1202.

[10] A.R. Mendoza, F. Corvo, A. Gómez, J. Gómez, Influence of the corrosion products of copper on its atmospheric corrosion kinetics in tropical climate, Corros. Sci. 46 (2004) 1189–1200.

doi:10.1016/j.corsci.2003.09.014.
[11] A.M. Pollard, R.G. Thomas, P.A. Williams, Connellite : stability relationships with other secondary copper minerals, 54 (1990) 425–430.
[12] G. Di Carlo, C. Giuliani, C. Riccucci, M. Pascucci, E. Messina, G. Fierro, M. Lavorgna, G.M. Ingo, Artificial patina formation onto copper-based alloys: Chloride and sulphate induced corrosion processes, Appl. Surf. Sci. 421 (2017) 120–127. doi:10.1016/j.apsusc.2017.01.080.
[13] J.T. Jambor, John L.; Dutrizac, John E.; Roberts, Andrew C.; Grice, Joel D.; Szymanski, Clinoatacamite, a new polymorph of Cu2(OH)3Cl, and its relationship to paratacamite and "anarakite," Can. Mineral. 34 (1996) 61–72.
[14] R.W. Revie, Uhlig ' S Corrosion Handbook the Electrochemical Society Series, 2011. doi:10.1002/9780470872864.ch39.
[15] L.S. Selwyn, N.E. Binnie, J. Poitras, M.E. Laver, D.A. Downham, Outdoor Bronze Statues: Analysis of Metal and Surface Samples, Stud. Conserv. 41 (1996) 205. doi:10.2307/1506541.
[16] M. Rita Perrone, A. Turnone, A. Buccolieri, G. Buccolieri, Particulate matter characterization at a coastal site in south-eastern Italy, J. Environ. Monit. 8 (2006) 183–190. doi:10.1039/B513306H.
[17] A. Buccolieri, G. Buccolieri, N. Cardellicchio, A. Dell'Atti, E.T. Florio, PM-10 and heavy metals in particulate matter of the province of Lecce (Apulia, Southern Italy), Ann. Chim. 95 (2005). doi:10.1002/adic.200590004.
[18] A. Buccolieri, A. Castellano, E. Degl'Innocenti, R. Cesareo, R. Casciaro, G. Buccolieri, EDXRF analysis of gold jewelry from the Archaeological Museum of Taranto, Italy, X-Ray Spectrom. 46 (2017). doi:10.1002/xrs.2761.
[19] A. Buccolieri, E. Degl'Innocenti, R. Cesareo, A. Castellano, G. Buccolieri, Non-invasive in-situ analysis of a wreath of gold leaves from the National Archaeological Museum of Taranto, Italy, Meas. J. Int. Meas. Confed. 126 (2018) 164–167. doi:10.1016/j.measurement.2018.05.063.
[20] G. Buccolieri, A. Buccolieri, P. Donati, M. Marabelli, A. Castellano, Nuclear Instruments and Methods in Physics Research B Portable EDXRF investigation of the patinas on the Riace Bronzes, Nucl. INSTRUMENTS METHODS Phys. 343 (2015) 101–109. doi:10.1016/j.nimb.2014.11.064.
[21] R.L. Frost, W. Martens, J. Theo Kloprogge, P.A. Williams, Raman spectroscopy of the basic copper chloride minerals atacamite and paratacamite: Implications for the study of copper, brass and bronze objects of archaeological significance, J. Raman Spectrosc. 33 (2002) 801–806. doi:10.1002/jrs.921.
[22] R.L. Frost, W.N. Martens, L. Rintoul, E. Mahmutagic, J.T. Kloprogge, Raman spectroscopic study of azurite and malachite at 298 and 77 K, J. Raman Spectrosc. 33 (2002) 252–259. doi:10.1002/jrs.848.
[23] R.L. Frost, P.A. Williams, W. Martens, P. Leverett, J.T. Kloprogge, Raman spectroscopy of basic copper(II) and some complex copper(II) sulfate minerals: Implications for hydrogen bonding, Am. Mineral. 89 (2004) 1130–1137. doi:10.2138/am-2004-0726.
[24] G. Bertolotti, D. Bersani, P.P. Lottici, M. Alesiani, T. Malcherek, J. Schlüter, Micro-Raman study of copper hydroxychlorides and other corrosion products of bronze samples mimicking archaeological coins, Anal. Bioanal. Chem. 402 (2012) 1451–1457. doi:10.1007/s00216-011-5268-9.
[25] R.L. Frost, R. Scholz, A. López, Y. Xi, C. Lana, Vibrational spectroscopy of the sulphate mineral sturmanite from Kuruman manganese deposits, South Africa, Spectrochim. Acta - Part A Mol. Biomol. Spectrosc. 133 (2014) 24–30. doi:10.1016/j.saa.2014.04.115.
[26] T. Catelani, G. Pratesi, M. Zoppi, Raman characterization of ambient airborne soot and associated mineral phases, Aerosol Sci. Technol. 48 (2014) 13–21. doi:10.1080/02786826.2013.847270.
[27] C. Brolly, J. Parnell, S. Bowden, Raman spectroscopy: Caution when interpreting organic carbon from oxidising environments, Planet. Space Sci. 121 (2016) 53–59. doi:10.1016/j.pss.2015.12.008.
[28] A. Coccato, J. Jehlicka, L. Moens, P. Vandenabeele, Raman spectroscopy for the investigation of carbon-based black pigments, J. Raman Spectrosc. 46 (2015) 1003–1015. doi:10.1002/jrs.4715.
[29] M. Schmidt, H.D. Lutz, Hydrogen bonding in basic copper salts: a spectroscopic study of malachite, Cu2(OH)2CO3, and brochantite, Cu4(OH)6SO4, Phys. Chem. Miner. 20 (1993) 27–32. doi:10.1007/BF00202247.
[30] M. Bouchard, D.C. Smith, Catalogue of 45 reference Raman spectra of minerals concerning research in art history or archaeology, especially on corroded metals and coloured glass, Spectrochim. Acta - Part A Mol. Biomol. Spectrosc. 59 (2003) 2247–2266. doi:10.1016/S1386-1425(03)00069-6.
[31] R.L. Frost, Raman spectroscopy of selected copper minerals of significance in corrosion, Spectrochim. Acta - Part A Mol. Biomol. Spectrosc. 59 (2003) 1195–1204. doi:10.1016/S1386-1425(02)00315-3.
[32] P. Makreski, G. Jovanovski, S. Dimitrovska, Minerals from Macedonia: XIV. Identification of some sulfate minerals by vibrational (infrared and Raman) spectroscopy, Vib. Spectrosc. 39 (2005) 229–239.

doi:10.1016/j.vibspec.2005.04.008.
[33] M.D. Lane, Mid-infrared emission spectroscopy of sulfate and sulfate-bearing minerals, Am. Mineral. 92 (2007) 1–18. doi:10.2138/am.2007.2170.
[34] K. Ben Mabrouk, T.H. Kauffmann, H. Aroui, M.D. Fontana, Raman study of cation effect on sulfate vibration modes in solid state and in aqueous solutions, J. Raman Spectrosc. 44 (2013) 1603–1608. doi:10.1002/jrs.4374.
[35] A. Coccato, D. Bersani, A. Coudray, J. Sanyova, L. Moens, P. Vandenabeele, Raman spectroscopy of green minerals and reaction products with an application in Cultural Heritage research, J. Raman Spectrosc. 47 (2016) 1429–1443. doi:10.1002/jrs.4956.

AUTHOR INFORMATION

ORCID ID:

Buccolieri Giovanni: http://orcid.org/0000-0001-8672-9238

Alfredo Castellano: http://orcid.org/0000-0002-3107-5836

Antonio Serra: http://orcid.org/0000-0003-3380-7751

Giorgio Zavarise: http://orcid.org/0000-0002-6340-0015

Buccolieri Alessandro: http://orcid.org/0000-0002-8657-9468

Caption of the Figures

Fig. 1. Images of the *Sant'Oronzo* statue (a) and degraded areas of copper *patinas* (b, c and d), of the Roman column (e, f and g) and the concrete base (h). The figure also shows the seven sampling points, which provided the samples analysed both with Raman and XRD.

Fig. 2. Typical Raman spectrum (a) and XRD pattern (b) of the green *patina* compared with brochantite standard.

Fig. 3. Typical Raman spectrum (a) and XRD pattern (b) of the dark *patina* compared with atacamite standard.

Fig. 4. Typical Raman spectrum (a) and XRD pattern (b) of the sample C04 compared with calcite standard.

Fig. S1. Image from above (a) and front (b) of the original nails of the *Sant'Oronzo* statue.

Fig. S2. Rivet fixing technique.

Fig. S3. Image of evidence of rivets on the statue.

Fig. S4. Image of the *Sant'Oronzo* statue in the room where it will be restored.

Fig. S5. XRD pattern of the sample C01.

Caption of the Tables

Table 1. ED-XRF analysis results of different *patinas* on the *Sant'Oronzo* statue.

Table 2. Description of the seven samples analysed by Raman spectroscopy and XRD and main compounds detected

Table 3. Raman peaks obtained from *patinas* on the *Sant'Oronzo* statue and their possible assignment.

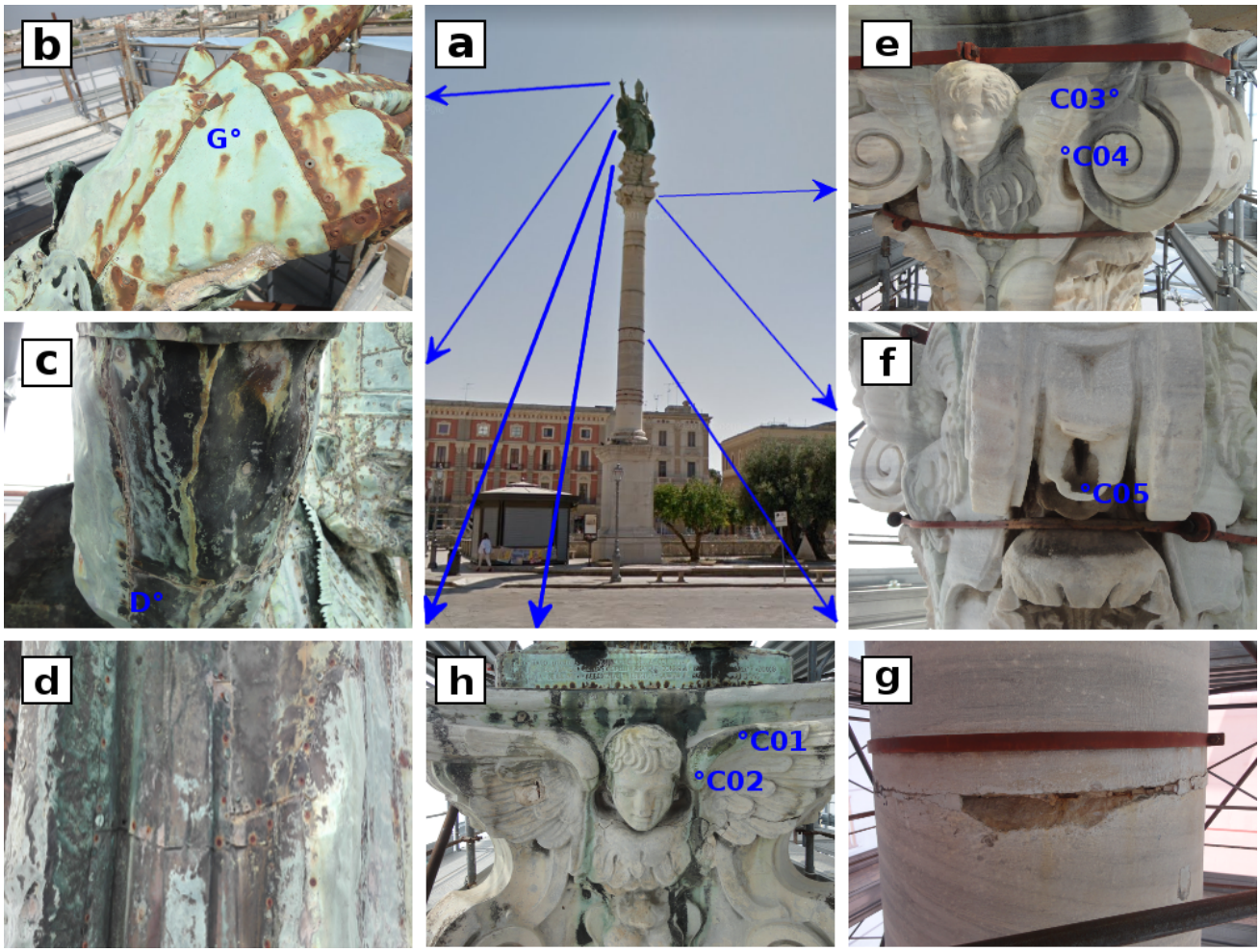

Fig. 1

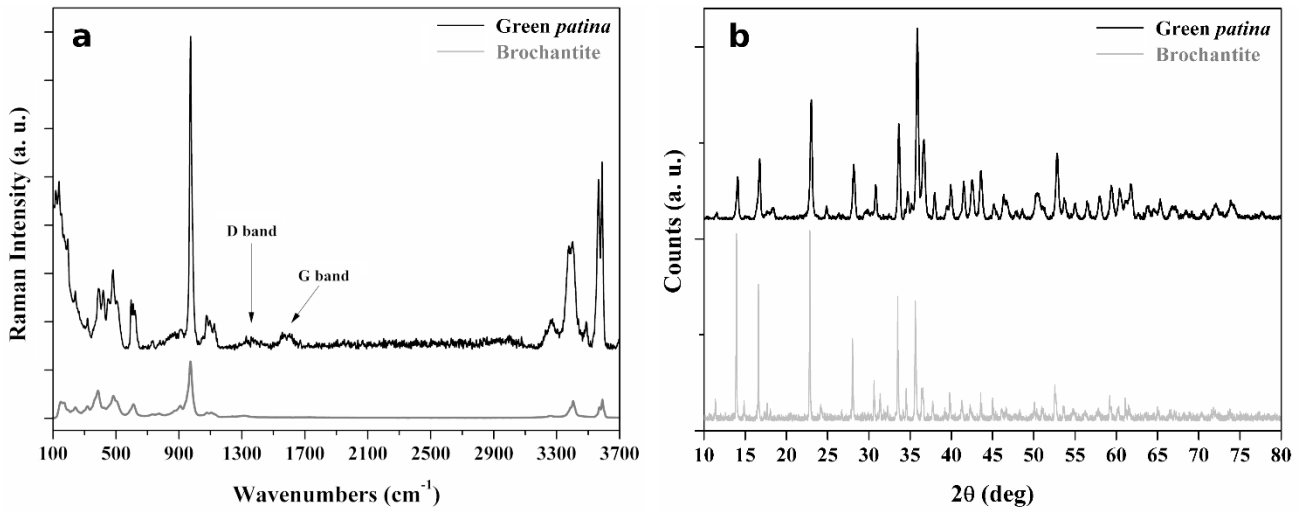

Fig. 2

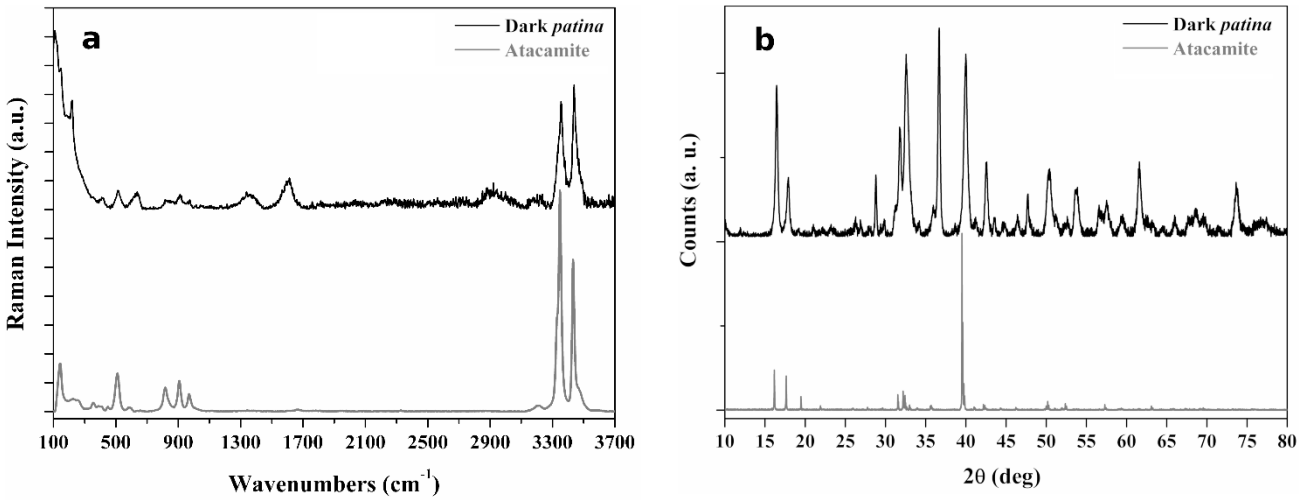

Fig. 3

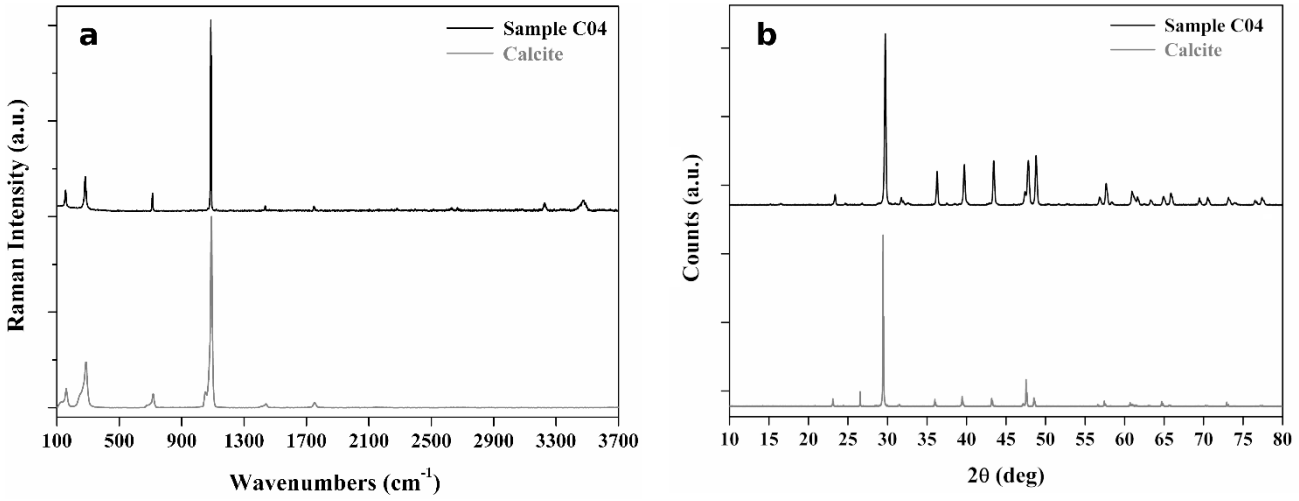

Fig. 4

Table 1

Sample	Description of sample	Cu	S	Cl	Fe
		(% wt)			
01	Right hand, green *patina* exposed to leaching	65±2	20±2	<0.5	<0.5
01*c*	Sample 01 *after cleaning*	89±2	2.5±0.5	<0.5	1.0±0.5
02	Right hand, red *patina* exposed to leaching	48.0±1.5	4.4±0.5	<0.5	23±2
03	Right hand, red dripping exposed to leaching	58±2	11.0±1.0	<0.5	4.5±0.5
04	Right hand, red sheet exposed to leaching	87±2	<0.5	<0.5	2.5±0.5
05	Right arm, dark *patina* sheltered area	50±2	<0.5	23±2	<0.5
06	Right arm, greenish dripping, sheltered area	49±2	17.0±1.5	3.5±0.5	4.0±0.5
07	Dark *patina* under the mantle, sheltered area	47±2	<0.5	20±2	<0.5
08	Hole on the arm	69±2	7.0±1.0	<0.5	10.0±1.0
09	Mantle, right side, green *patina*, flat surface	20±2	8.0±1.0	7.0±0.5	<0.5
10	Bottom right mantle, dark *patina*	45±2	<0.5	19.3±1.5	1.5±0.5
11	Right side, dark *patina*, sheltered area	48±2	<0.5	16.3±1.5	<0.5
12	Bottom right mantle, dark *patina* with red dripping	38±2	11.5±1.0	<0.5	1.5±0.5
13	Bottom right base, dark *patina*	41±2	5.0±0.5	14.0±1.5	<0.5
14	Right side, iron rod	<1.0	<0.5	<0.5	55±2
15	Brown *patina*, sheltered area	53±2	<0.5	11.0±1.0	<0.5
15*c*	Sample 15 *after cleaning*	92±2	<0.5	<0.5	<0.5
16	Right hand, original nail, exposed to leaching	56±2	<0.5	21±2	1.0±0.5
16*c*	Sample 16 *after cleaning*	90±2	<0.5	1.5±0.5	1.0±0.5
17	Original nail with green head	52±2	12.0±1.0	5.0±0.5	<0.5
17c	Sample 17 *after cleaning*	91±2	<0.5	<0.5	<0.5
18	Original nail with dark head	45±2	<0.5	21±2	<0.5
18*c*	Sample 18 *after cleaning*	91±2	<0.5	<0.5	<0.5
19	Right hand, recent red rivet, exposed to leaching	39±2	<0.5	1.0±0.5	10.0±1.0
19*c*	Sample 19 *after cleaning*	89±2	<0.5	<0.5	8.0±1.0
20	Right hand, red rivet, exposed to leaching	12.0±1.0	<0.5	<0.5	27±2

Table 2

Sample	Description of sample	Main compounds determined	
		by Raman	by XRD
G	Right hand, green sheet, exposed to leaching	Brochantite	Brochantite, Cuprite
D	Right arm, dark sheet, sheltered area	Atacamite	Atacamite, Cuprite
C01	Dark dripping on concrete pulvino, South side	Calcite	Calcite, Gypsum, Murdochite
C02	Green dripping on concrete pulvino, South side	Calcite	Calcite, Atacamite
C03	Dark dripping on Roman capital, West side	Calcite	Calcite, Murdochite
C04	Green dripping on Roman capital, West side	Calcite	Calcite
C05	Dark area on Roman capital (volute), North-West side	Gypsum	Gypsum

Table 3

Wavenumber (cm^{-1})	Suggested assignment
120 140	Cu−O bending
155	(Ca^{2+}, CO_3^{2-}) lattice modes
200	Cu−Cl bending
225	Cu−O bending
242	Cu−Cl bending
285	(Ca^{2+}, CO_3^{2-}) lattice modes
318 390 420	Cu−Cl stretching
450	SO_4^{2-} symmetric bending
485 506	Cu−O symmetric stretching
520	Cu−OH symmetric stretching
595 609 622	SO_4^{2-} anti-symmetric bending
625	Cu−O symmetric stretching
715	CO_3^{2-} symmetric stretching
808 825 910 975	OH deformation
975	SO_4^{2-} symmetric stretching
1075 1095 1125	SO_4^{2-} anti-symmetric stretching
1085	CO_3^{2-}symmetric stretching
1350	disorder carbon (*band D*)
1580	graphitic carbon (*band G*)
1435	CO_3^{2-} asymmetric stretching
1750	CO_3^{2-}symmetric stretching
3260 3375 3405 3490 3565 3585	Cu−OH hydroxyl stretching